Quantum Electronics **48** (3) 255–262 (2018) ©2018 Kvantovaya Elektronika and Turpion Ltd

https://doi.org/10.1070/QEL16526

Modelling of heating and photoexcitation of single-crystal silicon under multipulse irradiation by a nanosecond laser at 1.06 μm

D.S. Polyakov, E.B. Yakovlev

Abstract. **We report a theoretical study of heating and photoexcitation of single-crystal silicon by nanosecond laser radiation at a wavelength of 1.06 μm. The proposed physicomathematical model of heating takes into account the complex nonlinear dynamics of the interband absorption coefficient of silicon and the contribution of the radial heat removal to the cooling of silicon between pulses under multipulse irradiation, which allows one to obtain a satisfactory agreement between theoretical predictions of silicon melting thresholds at different nanosecond pulse durations and experimental data (both under single-pulse and multipulse irradiation). It is found that under irradiation by nanosecond pulses at a wavelength of 1.06 μm, the dynamic Burshtein–Moss effect can play an important role in processes of photoexcitation and heating. It is shown that with the regimes typical for laser multipulse microprocessing of silicon (the laser spot diameter is less than 100 μm, and the repetition rate of pulses is about 100 kHz), the radial heat removal cannot be neglected in the analysis of heat accumulation processes.**

Keywords: *nanosecond laser pulses, single-crystal silicon, multipulse regime, dynamic Burshtein–Moss effect.*

1. Introduction

Exposure of single-crystal silicon and structures based on it to nanosecond laser pulses can be used for producing various surface microreliefs [1, 2], for annealing ion-implanted layers [3, 4], for obtaining silicon nanoparticles [5], etc. In this case, use is usually made of visible and UV lasers. A wavelength of 1.06 μm is not so popular because of a low initial absorption coefficient, which is only 10–30 cm^{-1} [6]. However, due to a number of nonlinear effects during the interaction process, the absorption coefficient can increase by several orders of magnitude, which makes it possible to process single-crystal silicon with nanosecond pulses at a wavelength of 1.06 μm. Nevertheless, until recently the studies carried out in this spectral region were of a fundamental rather than an applied nature (see, for example, [7–9]). The appearance and widespread introduction of ytterbium fibre lasers with unquestionable technological advantages (such as high productivity and efficiency, long service life, reliability, etc.) raise the question of whether they should be used for processing single-crystal silicon and structures based on it. For example, the authors of Refs [10, 11] demonstrated their high efficiency (in combination with a rather high quality of processing) in performing simple technological operations of hole drilling and scribing. A fibre laser can also be successfully used to form a relief with an antireflection effect [12] and to generate silicon nanoparticles [13]. A number of interesting results related to the formation of the microrelief and structural changes at the silicon/silicon dioxide interface were obtained in [14, 15] when studying the effect of radiation from an ytterbium fibre laser on silicon oxide structures widely used in microelectronics. The possibility of a controlled change in the characteristics of the elements of silicon integrated circuits was demonstrated in [16] under similar irradiation conditions.

Practical interest in the problem of silicon irradiation by nanosecond pulses at a wavelength of 1.06 μm contributes to the development of physicomathematical models and laser initiated processes, primarily optical (radiation absorption) and thermophysical ones. Here, in our opinion, it is possible to distinguish two specific aspects of the action, insufficiently studied in the scientific literature.

The first aspect is related to the relatively complex dynamics of the absorption coefficient α of silicon exposed to radiation at a wavelength of 1.06 μm. The small initial value of α is due to the fact that the wavelength of 1.06 μm lies on the edge of the region of intrinsic absorption of silicon. On the one hand, under sufficiently intense laser irradiation, an increase in α results from the heating of the lattice, which leads to a decrease in the width of the forbidden band and, accordingly, to the involvement of a larger number of levels in the interband transitions, as well as to an increase in the probability of indirect optical transitions due to an increase in the phonon concentration. In addition, an increase in the concentration of photoexcited carriers leads to an increase in the intraband absorption coefficient. On the other hand, under this irradiation there occur processes that contribute to a decrease in the interband absorption coefficient and prevent the growth of the electron–hole plasma concentration. The fact is that strong photoexcitation of silicon will lead to the state filling by carriers near the extrema of the bands, which, with an insignificant excess of the width of the forbidden band (even with allowance for its temperature narrowing) by the energy of the quantum, can cause a noticeable decrease in the interband transitions and a decrease in the interband absorption coefficient. The described phenomenon is called the dynamic Burstein–Moss effect (DBME) and is usually ignored when constructing nanosecond impact models for single-crystal silicon at a wavelength of 1.06 μm (see, for example, [17–23]). It should be noted that the important role of this effect was noted in an early paper [24] for the case of millisecond irradiation (see also [25]). It was also demonstrated that a single-

D.S. Polyakov, E.B. Yakovlev ITMO University, Kronverskii prosp. 49, 197101 St. Petersburg, Russia;
e-mail: polyakovdmitry1988@gmail.com

Received 13 September 2017; revision received 29 December 2017
Kvantovaya Elektronika **48** (3) 255–262 (2018)
Translated by I.A. Ulitkin

crystal silicon wafer can be used as a saturable absorber in neodymium lasers [25]. Under nanosecond exposures, the concentration of photoexcited carriers is much greater than under millisecond irradiations, and so it is logical to expect that the DBME can influence the processes of heating and photoexcitation of silicon in this case. However, there are no such estimates.

The second aspect is related to the peculiarities of multipulse irradiation. Fibre lasers operate at high pulse repetition rates (tens to hundreds of kilohertz), at which the effects of heat accumulation become important. Existing models of multipulse irradiation for the specified frequency range have a number of drawbacks. For example, the model from Ref. [19] is one-dimensional, although it is obvious that in the case of multipulse exposure, radial heat removal can be essential. In a later model [20], radial heat removal is taken into account; however, the multipulse regime was not investigated. In addition, in both models [19, 20], the dynamics of the electronic subsystem of the semiconductor is completely ignored. The problem with three-dimensional heat removal was analysed in [14]; nevertheless, the complex dynamics of the interband absorption coefficient was not taken into account, an explicitly overestimated value of the absorption cross section on free carriers was used and the nonlinearity of the thermophysical properties of silicon was ignored.

Thus, the aim of this work is to analyse multipulse heating of single-crystal silicon by nanosecond pulses at a wavelength of 1.06 μm at their repetition rates of 1–1000 kHz in the framework of the model that takes into account both different mechanisms of the absorption coefficient nonlinearity and the contribution of the radial heat removal to the heat accumulation effect from pulse to pulse.

2. Basic equations describing silicon heating and photoexcitation by nanosecond pulses

The dynamics of heating and photoexcitation of single-crystal silicon by nanosecond laser pulses will be described by a system of coupled equations of heat conduction and diffusion of photoexcited carriers, as well as by an equation describing the attenuation of radiation during its propagation inside a material. Together with the initial and boundary conditions in a cylindrical coordinate system, this system will have the form:

$$c_s(T_s)\frac{\partial T_s}{\partial t} = \frac{1}{r}\frac{\partial}{\partial r}\left(rk_s(T_s)\frac{\partial T_s}{\partial r}\right) + \frac{\partial}{\partial z}\left(k_s(T_s)\frac{\partial T_s}{\partial z}\right) + q_T(T_s, n_e), \quad (1)$$

$$\frac{\partial n_e}{\partial t} = \frac{1}{r}\frac{\partial}{\partial r}\left(rD(T_s)\frac{\partial n_e}{\partial t}\right) + \frac{\partial}{\partial z}\left(D(T_s)\frac{\partial n_e}{\partial z}\right) + q_n(T_s, n_e), \quad (2)$$

$$\frac{\partial q}{\partial z} = -[\alpha_{vc}(T_s, n_e) + \alpha_n(T_s, n_e)]q, \quad (3)$$

$$\left.\frac{\partial T_s}{\partial z}\right|_{z=0} = \left.\frac{\partial T_s}{\partial z}\right|_{z=L} = 0, \quad \left.\frac{\partial T_s}{\partial r}\right|_{r=0} = \left.\frac{\partial T_s}{\partial r}\right|_{r\to\infty} = 0, \quad (4)$$

$$\left.\frac{\partial n_e}{\partial z}\right|_{z=0} = \left.\frac{\partial n_e}{\partial z}\right|_{z=L} = 0, \quad \left.\frac{\partial n_e}{\partial r}\right|_{r=0} = \left.\frac{\partial n_e}{\partial r}\right|_{r\to\infty} = 0, \quad (5)$$

$$q|_{z=0} = (1 - R_s)q_0, \quad (6)$$

$$T_s|_{t=0} = T_0, \quad n_e|_{t=0} = n_0, \quad (7)$$

where $T_s = T_s(r, z, t)$ is the temperature of single-crystal silicon; $n_e = n_e(r, z, t)$ is the concentration of photoexcited carriers; $q = q(r, z, t)$ is the radiation power density; c_s is the specific heat capacity of silicon; k_s is the coefficient of thermal conductivity; D is the carrier diffusion coefficient; q_T is a volume heat source; q_n is the volume carrier source; α_{vc} is the interband absorption coefficient; α_n is the coefficient of intraband absorption on free carriers; $R_s = 0.33$ is the reflection coefficient at a wavelength of 1.06 μm [19]; $q_0 = q_0(r, t)$ is the power density of the incident laser radiation; L is the thickness of the silicon wafer; $T_0 = 293$ K and $n_0 = 10^{12}$ cm^{-3} are the initial temperature of silicon and the carrier concentration, respectively; r and z are the radial and axial coordinates; and t is the time. It is assumed that the laser beam has an axial symmetry and irradiation is carried out without its displacement over the surface.

The volume sources in formulas (1) and (2) are determined in accordance with the relations:

$$q_n(T_s, n_e) = \frac{\alpha_{vc}(T_s, n_e)q}{\hbar\omega} - \left(\gamma n_e^3 + \frac{n_e}{\tau_r}\right), \quad (8)$$

$$q_T(T_s, n_e) = \left\{\alpha_{vc}(T_s, n_e)\left[1 - \frac{E_g(T_s, n_e)}{\hbar\omega}\right] + \alpha_n(T_s, n_e)\right\}q + \left(\gamma n_e^3 + \frac{n_e}{\tau_r}\right)E_g(T_s, n_e), \quad (9)$$

where $\hbar$ is the reduced Planck constant; ω is the frequency of the incident radiation; $\gamma = 1.2 \times 10^{-31}$ cm^6 s^{-1} is the Auger recombination coefficient [26]; $\tau_r \approx 10^{-6}$ s is the characteristic time of nonradiative recombination [25]; and E_g is the width of the forbidden band of silicon, which depends both on the silicon temperature and on the concentration of free carriers (see below). The first term in Eqn (8) is associated with carrier generation during interband absorption, and the excess energy ($\sim\hbar\omega - E_g$) is transferred to the lattice due to the electron–phonon interaction. The second term in (8) is related to the processes of nonradiative recombination and Auger recombination. In this case, the energy $\sim E_g$ will be released in the lattice. While no energy is directly released in the lattice during the Auger recombination, the corresponding term in the expression for the thermal source (9) is still present, since the energy obtained by the third carrier is practically instantaneously transferred to the lattice by means of the electron–phonon interaction. Equation (9) also contains a term associated with absorption on free carriers.

To describe the temperature dependences of the heat capacity and thermal conductivity of silicon, we used the approximations of experimental data known from the literature (see, for example, [19] and references therein):

$$c_s(T_s) = 1.6\exp(2.375 \times 10^{-4}T_s) \ [\text{J cm}^{-3}\ \text{K}^{-1}], \quad (10)$$

$$k_s(T_s) = \begin{cases} 1521T_s^{-1.226}, & T_s < 1200\ \text{K} \\ 8.98T_s^{-0.502}, & T_s \geqslant 1200\ \text{K} \end{cases} \ [\text{W cm}^{-1}\ \text{K}^{-1}]. \quad (11)$$

The coefficient of ambipolar diffusion of carriers is calculated from the formula

$$D = \frac{2D_eD_h}{D_e + D_h},$$

where the diffusion coefficients of electrons (D_e) and holes (D_h) were estimated as $D_{e,h} \approx v_{e,h}^2/(3\gamma_{ph})$ (here, $v_{e,h}$ are the average thermal velocities of electrons and holes, and γ_{ph} is the frequency of collisions of carriers with a lattice).

When silicon is heated to the melting point and energy absorption corresponding to the specific melting heat, there occurs a phase transition accompanied by a change in the optical and thermophysical properties of silicon. As is known, during melting it undergoes a semiconductor–metal transition, while the absorption becomes superficial, and the reflection coefficient increases substantially. To describe the temperature field in the melt, the heat conduction equation is solved, and the motion of the melting front is described in the framework of the classical Stefan problem:

$$c_1 \frac{\partial T_1}{\partial t} = \frac{1}{r}\frac{\partial}{\partial r}\left(rk_1(T_1)\frac{\partial T_1}{\partial r}\right) + \frac{\partial}{\partial z}\left(k_1(T_1)\frac{\partial T_1}{\partial z}\right), \quad (12)$$

$$-k_1\frac{\partial T_1}{\partial n_{sl}} + k_s\frac{\partial T_s}{\partial n_{sl}} = v_{sl}L_{sl}, \quad (13)$$

$$T_s\big|_{r=r_{sl}, z=z_{sl}} = T_1\big|_{r=r_{sl}, z=z_{sl}} = T_m, \quad (14)$$

$$-k_l\frac{\partial T_1}{\partial z}\Big|_{z=0} = (1-R_1)q_0, \quad (15)$$

where $T_1 = T_1(r,z,t)$ is the temperature of the silicon melt; $c_1 = 2.65$ J cm^{-3} K^{-1} is the heat capacity of the melt [19]; k_1 is the thermal conductivity of the melt; v_{sl} is the velocity of the interphase boundary movement; $L_{sl} = 3.8 \times 10^3$ J cm^{-3} is the specific melting heat [19]; n_{sl} is the normal to the melting front; z_{sl} and r_{sl} are the coordinates of the interphase boundary; $R_1 = 0.8$ is the reflection coefficient of the melt [19]; and $T_m = 1685$ K is the melting temperature of silicon.

For the heating stage, in which both the solid and liquid phases of silicon are present, in the region unoccupied by the melt the heat conduction equation (1) is solved, which, in addition to the boundary conditions (4), is supplemented with conditions (13) and (14) acting at the interphase boundary. Since the silicon melt is opaque to incident radiation, $q = 0$ in the region under the melt layer. It is also assumed that the carrier flux at the interphase boundary is absent. In the region where there is a melt, only equation (12) with boundary conditions (13)–(15) is solved, and it is assumed that immediately after solidification of the melt, the carrier concentration becomes equal to the equilibrium concentration in solid silicon at the melting temperature.

3. Model of the dependence of the absorption coefficient of single-crystal silicon at a wavelength of 1.06 μm on the concentration of photoexcited carriers and temperature

As was already noted, the change in the interband absorption coefficient of silicon, α_{vc}, at a wavelength of 1.06 μm is related to a temperature narrowing of the forbidden band width, to an increase in the phonon concentration (which increases the probability of indirect transitions), as well as to the DBME. Under these conditions, the coefficient α_{vc} entering into equations (3), (8) and (9) will be determined by an expression of the form (see [27], p. 236)

$$\alpha_{vc}(T_s,n_e) = A\Bigg\{[N(T_s)+1]\int_{E_g(T_s,n_e)}^{\hbar(\omega-\Omega)}\{f_v[E-\hbar(\omega-\Omega)] - f_c(E)\} \times\sqrt{E-E_g(T_s,n_e)}\sqrt{\hbar(\omega-\Omega)-E} + N(T_s)\int_{E_g(T_s,n_e)}^{\hbar(\omega-\Omega)}\{f_v[E-\hbar(\omega+\Omega)] - f_c(E)\} \times\sqrt{E-E_g(T_s,n_e)}\sqrt{\hbar(\omega+\Omega)-E}\,\mathrm{d}E\Bigg\}, \quad (16)$$

where A is a constant coefficient, determined from the experimental data;

$$N(T_s) = \left[\exp\left(\frac{\hbar\Omega}{k_B T_s}\right) - 1\right]^{-1}$$

is the occupation number of phonons with energy $\hbar\Omega$; k_B is the Boltzmann constant;

$$f_{c,v}(E, T_s, n_e) = \left[\exp\left(\frac{E-\mu_{c,v}(T_s,n_e)}{k_B T_s}\right) + 1\right]^{-1}$$

are the quasi-equilibrium distribution functions of valence electrons and conduction electrons in energy; $\mu_{c,v}$ are the chemical potentials, determined from the normalisation conditions

$$\int_{E_g}^{\infty} f_c(E)g_c(E)\mathrm{d}E = n_e, \quad \int_{E_0}^{0} f_v(E)g_v(E)\mathrm{d}E = n_v - n_e;$$

n_v is the maximum concentration of valence electrons in silicon; and the energy is measured from the ceiling of the valence band. The densities of the $g_{c,v}$ levels are found from formulas

$$g_c(E) = \frac{\sqrt{2}\,m_c^{3/2}}{\pi^2\hbar^3}\sqrt{E-E_g}, \quad (17)$$

$$g_v(E) = \frac{\sqrt{2}\,m_v^{3/2}}{\pi^2\hbar^3}\sqrt{-E}, \quad (18)$$

where $m_c = 1.08m_0$; $m_v = 0.6m_0$ are the effective masses of the density of states in silicon [6]; and m_0 is the electron mass.

A decrease in the width of the forbidden band is due to the heating of the lattice and to the generation of an electron–hole plasma:

$$E_g(T_s,n_e) = E_g(0,0) - A_T N(T_s) - A_n\sqrt[3]{n_e}, \quad (19)$$

where A_T is the Fan parameter; $A_n = 1.5 \times 10^{-8}$ eV cm^{-1} [28]. The allowance for the temperature contribution to a decrease in E_g corresponds to the Fan model [29]. The values of the parameters $E_g(0,0) = 1.17$ eV, $A_T = 0.24$ eV and $\hbar\Omega = 0.054$ eV were chosen on the basis of the agreement with the experimental dependence $E_g(T_s,n_0)$ (see [30], p. 465) (Fig. 1a) and the experimental dependence $\alpha_{vc}(T_s,n_0)$ given in [31] (Fig. 1b). The value of the parameter A in formula (16) was determined from the initial value $\alpha_{vc}(T_0,n_0) \approx 12$ cm^{-1}. Figure 1b also shows the temperature dependence $\alpha_{vc}(T_s,n_e = 10^{20}$ cm$^{-3})$. It can be seen that at a concentration typical for nanosecond irradiation of silicon [25], there is a noticeable decrease in α_{vc} at $T_s < 900$ K, related to the DBME; however, at large temperatures the difference is small. Thus, to answer

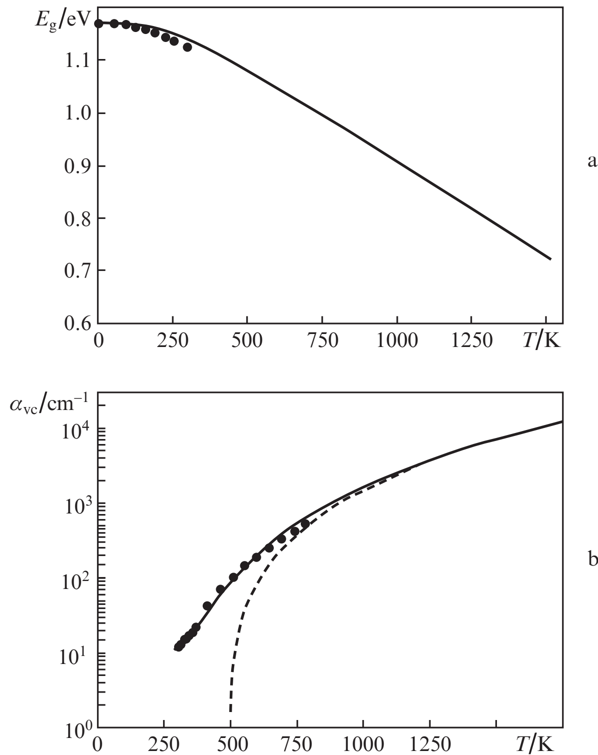

Figure 1. Dependences of (a) silicon forbidden bandwidth and (b) interband absorption coefficient on temperature; (a) points show the experimental data [30], and solid curve – approximation by formula (19); (b) points show the experimental data [31], solid curve – calculation by formula (16) for $n_e = n_0$, and dashed curve – calculation by formula (16) for $n_e = 10^{20}$ cm^{-3}.

the question about the role of the DBME, it is necessary to consider the situation in dynamics.

The free carrier absorption coefficient α_n is calculated from the Drude model. For $\omega > \omega_p$, $\omega > \gamma_{ph}$ (ω_p is the plasma frequency), according to [32]

$$\alpha_n(T_s, n_e) = \sigma(T_s) n_e, \tag{20}$$

where

$$\sigma(T_s) = \frac{e^2 \gamma_{ph}(T_s)}{\varepsilon_0 n m_{opt} c \omega^2};$$

σ is the absorption cross section on free carriers; e is the electron charge; ε_0 is the electric constant; c is the speed of light; n = 3.6 is the refractive index of silicon [6]; m_{opt} = $0.15m_0$ is the reduced optical mass of the carriers [33]; and $\gamma_{ph}(T_s) = \gamma_{ph}(T_0) \times T_s/T_0$ is the frequency of collisions of carriers with phonons. The choice of $\gamma_{ph}(T_0) \approx 8 \times 10^{13}$ s^{-1} makes it possible to match the value of the absorption cross section at room temperature with the experimental value $\sigma(T_0) \approx 5 \times 10^{-18}$ cm^2 [34].

4. Experimental determination of the threshold densities of the melting flux under nanosecond laser irradiation

Direct measurement of the temperature to which silicon is heated under nanosecond laser irradiation (including in the multipulse regime) is rather difficult; therefore, to verify the adequacy of the proposed model, it is reasonable to use the experimental dependences of the threshold energy densities of the melting on the pulse duration, on the number of pulses, on the pulse repetition rate, etc.

As a source of radiation during the experiments, we used a nanosecond ytterbium fibre laser generating pulses of 4–200 ns duration at a repetition rate from 2 to 100 kHz. Samples were 400-μm-thick wafers of KEF 4.5 brand single-crystal silicon with a crystallographic orientation of the surface (100). The intensity distribution along the beam cross section and its diameter in the processing plane were determined using a Beamage CCD23 beam profiling camera. Radiation having a transverse Gaussian intensity profile was focused into a spot with a radius of 35 μm at the e^{-1} level. In the case of multipulse irradiation, the number of pulses in the series was monitored with a high-speed photodiode.

The melting of the silicon surface (under single-pulse and multipulse irradiation) was recorded by the formation of a characteristic microrelief (shown in Fig. 2), whose appearance is usually associated with the action of thermocapillary forces in an inhomogeneously heated molten bath (see, for example, [35]). The energy density at the centre of the beam was taken as the melting threshold, at which the region in the central part of the beam melts; its radius is $\sim 0.3r_0$ (i.e., about 11 μm at r_0 = 35 μm). Note that at lower energy densities, the presence of the microrelief cannot be fixed (i.e., in fact, in our work, the threshold for the formation of the microrelief, shown in Fig. 2, is taken as the melting threshold). Of course, this method for determining the melting thresholds does not look quite rigorous, but the threshold energy densities determined in this way are in good agreement with the data obtained by the method based on measuring the jump in the reflection coefficient during the melting of silicon [36].

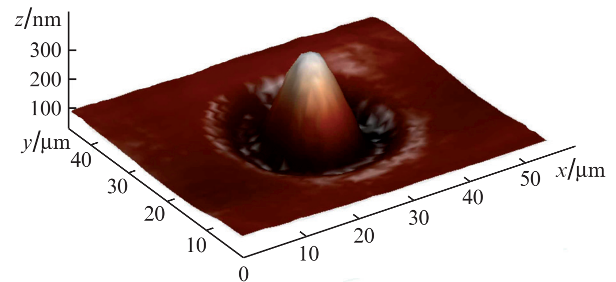

Figure 2. Microrelief of the silicon surface formed under nanosecond multipulse irradiation (irradiation regime: Q = 1.4 J cm^{-2}, t_p = 14 ns, r_0 = 35 μm, f = 99 kHz and number of pulses $N_p \sim 100$).

5. Analysis of heating and photoexcitation of silicon exposed to single pulses

The system of equations (1) and (2) describing the heating of silicon in the solid phase was analysed numerically using a locally one-dimensional implicit scheme (see [37], p. 332). Since when the silicon is heated in the solid phase under the conditions considered, the heat source is volumetric, the melting of the surface layer was modelled as follows. When a temperature equal to the melting temperature was reached on the silicon surface, its growth ceased until the moment of energy absorption equal to the corresponding specific melting heat. After this, it was assumed that the surface layer

melted, and the heat source was transferred to the surface. Further, in the region occupied by the melt, Eqn (12) was solved (also using a locally one-dimensional implicit scheme). At the cooling stage, in order to accelerate the calculations, we used a coarser computation grid and increased the time step.

When performing numerical calculations, it was assumed that the space–time structure of the pulse is described by the formula

$$q_{\mathrm{p}}(r,t) = \frac{Q}{t_0^2} t \exp\left(-\frac{t}{t_0}\right) \exp\left(-\frac{r^2}{r_0^2}\right), \quad (21)$$

where Q is the energy density; r_0 is the beam radius at the e^{-1} level; and t_0 is the duration of the leading edge of the pulse (when considering the action of single pulses $q_0 = q_{\mathrm{p}}$). The FWHM pulse duration is $t_{\mathrm{p}} \approx 2.5t_0$. The temporal shape of the pulse, described by formula (21), corresponds quite well to the actual pulse shape of the fibre laser used in the experiment.

Figure 3 shows the time dependence of the concentration of photoexcited carriers and the temperature of silicon on the surface at the centre of the beam upon irradiation by a 14-ns pulse with $Q = 3.3$ J cm^{-2}, close to the melting threshold. It is seen that the maximum carrier concentration is about 2×10^{20} cm^{-3}. A specific feature typical for the action at a wavelength of 1.06 μm is that the main contribution to surface heating is provided by the trailing edge of the pulse, and the maximum temperature is reached when the intensity of the heating pulse becomes approximately 30 times smaller than the maximum one (i.e., practically after the end of the pulse). This is due to a strong positive feedback between heating, photoexcitation and absorption of silicon. Figure 4, in addition to the pulse envelope, shows the time dynamics of the interband absorption coefficients α_{vc} (with and without the DBME) and the absorption coefficient on free carriers α_{n} near the surface at the centre of the beam (the irradiation regime is the same as in Fig. 3). One can see that α_{n} increases comparatively rapidly up to the 12th nanosecond and exceeds α_{vc} by more than an order of magnitude. At the trailing edge of the pulse, there is a rapid increase in the interband absorption coefficient, which becomes larger than the absorption coefficient on free carriers.

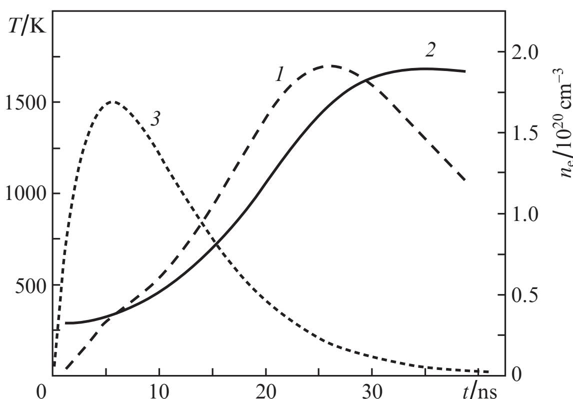

Figure 3. Typical time dependences of (*1*) carrier concentration and (*2*) silicon temperature on the surface at the beam centre under irradiation with a nanosecond pulse at a wavelength of 1.06 μm; (*3*) temporal shape of the pulse (irradiation regime is described in the text).

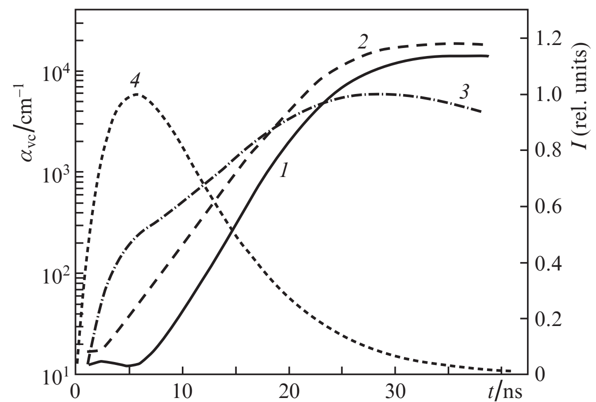

Figure 4. (*1*, *2*) Interband absorption coefficient calculated (*1*) with and (*2*) without the DBME and (*3*) absorption coefficient on free carriers vs. time; (*4*) pulse shape.

In calculations that do not take into account the DBME, the interband absorption coefficient at the initial stages of the pulse action is more than twice the coefficient calculated with allowance for the DBME. It is worth noting that the difference in estimates here is greater than in Fig. 1b, since the absorption coefficients calculated for identical carrier concentrations are compared (the carrier concentration contributes to the narrowing of the band gap and leads to an additional increase in the absorption coefficient calculated without taking the DBME into account). The difference in the model predictions is illustrated in Fig. 5a, which shows the dependences of the maximum lattice temperature on the

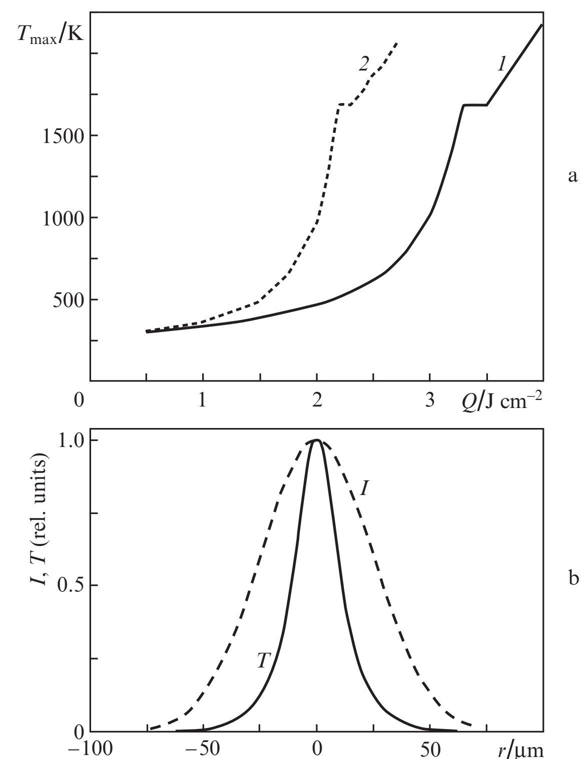

Figure 5. (a) Dependences of the maximum silicon temperature on the energy density of the pulse – calculation (*1*) with and (*2*) without the DBME taken into account and (b) radial distribution of the temperature field.

energy density of the pulse (at t_p = 14 ns). It can be seen that the predictions of the models can differ manifold. However, the behaviour of the $T_{max}(Q)$ dependence is preserved – in both cases the temperature increases rapidly with increasing energy density. It turns out that under the dome-shaped spatial intensity distribution (in particular, Gaussian) the spatial temperature distribution is much narrower (Fig. 5b), which is caused by a positive feedback between the temperature and the absorption coefficient, the distribution of which over the beam cross section is highly nonuniform. As can be seen from Fig. 5b, the spatial width of the temperature distribution is approximately two times smaller than the beam diameter (in estimates with respect to FWHM).

Figure 6 shows the calculated (with allowance for the DBME) and experimental dependences of the threshold density of the melting energy on the pulse duration (calculation was made for r_0 = 35 μm, at which heating by a single nanosecond pulse can be considered only with allowance for the heat removal into the depth). It can be seen that the agreement between them is quite satisfactory, and this confirms the validity of the considered approach to simulation of the processes of heating and photoexcitation of silicon by nanosecond pulses at a wavelength of 1.06 μm.

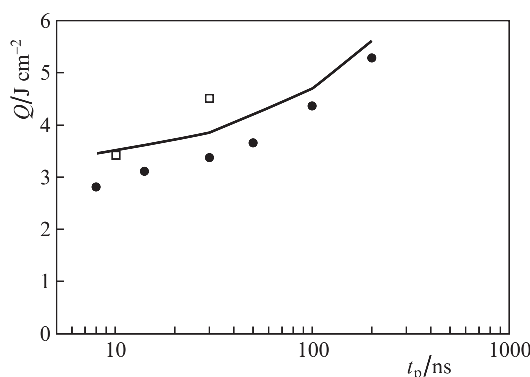

Figure 6. Experimental (points) and theoretical (curve) dependences of the threshold energy density of the melting on the pulse duration {(●) present work, (□) works [17, 36]}.

6. Analysis of heating and photoexcitation of silicon exposed to multiple pulses

In the case of multipulse irradiation, the function q_0 entering the boundary condition (6) will be determined by the formula

$$q_0(r,t) = \sum_{i=0}^{N_p-1} q_p(r, t - \mathrm{i}f^{-1}) \tag{22}$$

(f is the repetition rate of pulses, and N_p is the number of pulses).

From the simplest thermophysical considerations it follows that the degree of influence of the radial heat removal will depend on the beam diameter. Estimates show that for laser beam diameters typical for microprocessing ($2r_0$ ~ 10–100 μm), the contribution of the radial heat removal cannot be neglected in the analyses of multipulse heating. Thus, for example, Fig. 7 shows the silicon surface temperature as a function of time under irradiation by a series of 14-ns pulses with an energy density Q = 1.4 J cm^{-2} and r_0 = 35 μm at f = 99 kHz, calculated with and without allowance for the radial heat removal. As can be seen from the figure, the radial heat removal plays an important role in multipulse processing, and in analysing heating in one-dimensional models the temperature estimates can be significantly overestimated. It is also seen that at a given pulse repetition rate the material does not completely cool between the pulses and the heat accumulation effect takes place. Note that, since the carrier lifetime $\tau_r \ll f^{-1}$, there is no accumulation of carrier concentration from pulse to pulse. The maximum temperature reached during a pulse, when heating occurs in the solid phase, increases with time nonlinearly. When melting starts, the rate of growth of the maximum temperature from pulse to pulse slows down. This is explained by the fact that part of the energy supplied is now spent to advance the melting front to the depth and also by an increase in the reflection coefficient of the melt.

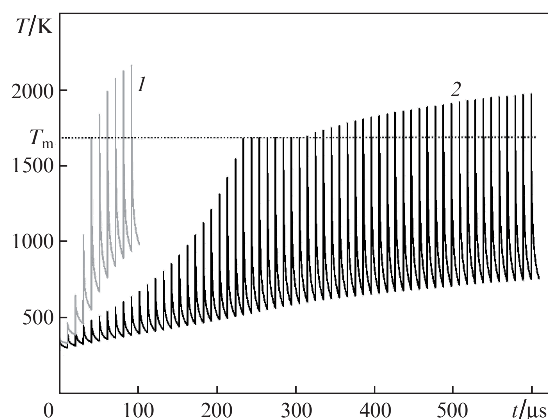

Figure 7. Dependences of the silicon surface temperature on time under multipulse irradiation, calculated (*1*) without and (*2*) with the radial heat removal taken into account (T_m is the melting temperature of silicon).

Figure 8a shows the dependence of the threshold number of pulses required for melting on the repetition rate of pulses with an energy density Q = 1.4 J cm^{-2} (t_p = 14 ns, r_0 = 35 μm). As can be seen from the figure, the heat accumulation effects become noticeable at repetition rates exceeding 30–40 kHz. Figure 8b demonstrates the dependence of the threshold number of pulses required for the melting of the silicon surface at Q = 1.4 J cm^{-2} (t_p = 14 ns, f = 99 kHz) on the beam radius. One can see that in the range r_0 > 50 μm, an increase in the beam radius does not lead to a change in the threshold number of pulses. However, in the range r_0 < 50 μm, a decrease in the beam radius causes a rapid increase in N_p, which indicates a large contribution of the radial heat flux to the cooling of silicon between pulses.

Figure 9 presents the calculated and experimental dependences of the threshold energy density on the number of 14- and 100-ns pulses with a repetition rate of 99 kHz. One can see that the coincidence of the calculated and experimental data in both cases is completely satisfactory. Thus, allowance for the radial heat removal in the model is of fundamental importance.

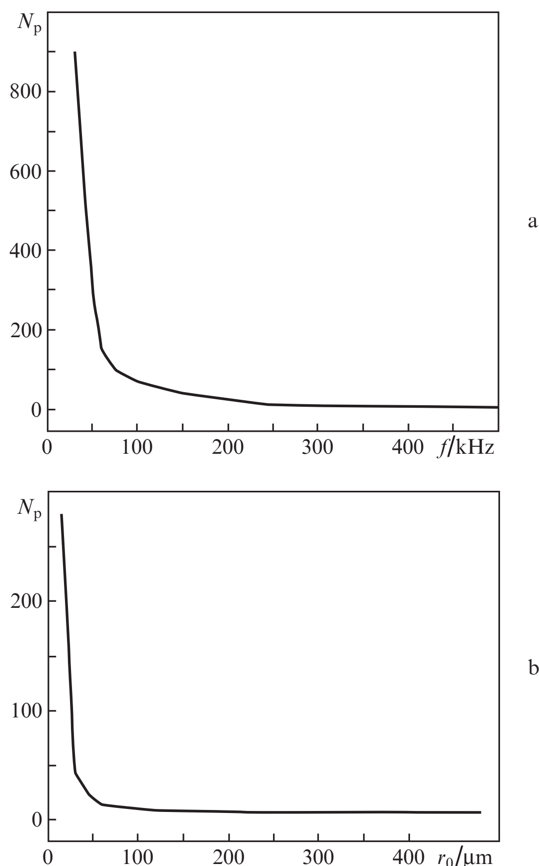

Figure 8. Dependences of the threshold number of pulses on (a) their repetition rate and (b) the beam radius.

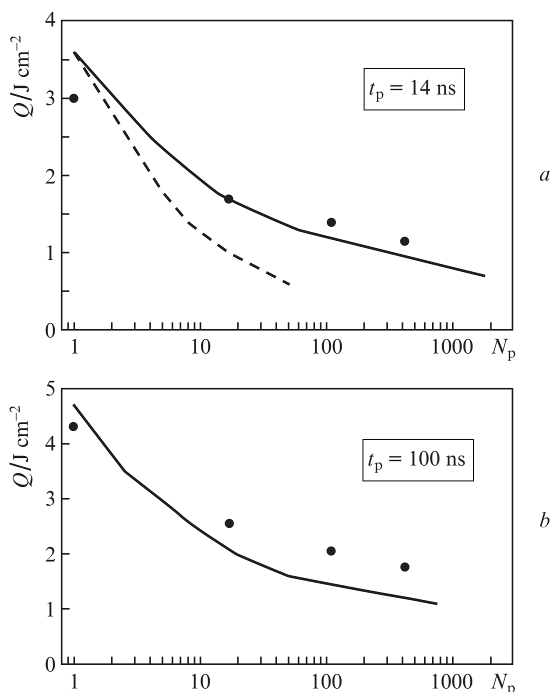

Figure 9. Dependences of the threshold energy density on the number of pulses at f = 99 kHz for t_p = (a) 14 and (b) 100 ns [the points are the experiment (present work), the solid curve is the calculation taking into account the radial heat removal, and the dashed curve is calculation neglecting the radial heat removal).

7. Conclusions

We have proposed a heating model taking into account photoexcitation of single-crystal silicon by nanosecond laser pulses at a wavelength of 1.06 μm, which lies on the boundary of the intrinsic absorption. It is shown that the dynamic Burstein – Moss effect plays an important role in the complicated nonlinear dynamics of change in the interband absorption coefficient, α_{vc}; therefore, ignoring this effect leads to a several-fold overestimate of α_{vc}. Despite this, the positive feedback between the heating and the absorption coefficient is significant, which, in the case of a Gaussian intensity distribution in the laser beam, results in that the spatial temperature distribution width is considerably smaller than the beam diameter. This feature is characteristic precisely for the irradiation by short pulses at a wavelength of 1.06 μm. It is found that with the regimes typical for laser multipulse microprocessing of silicon, one cannot neglect the radial heat removal in the analysis of heat accumulation processes. The melting thresholds calculated within the framework of the proposed model are in satisfactory agreement with the experimental data for single-pulse and multipulse nanosecond exposures.

Acknowledgements. The work was supported by the Ministry of Education and Science of the Russian Federation [Agreement No. 14.578.21.0197 (RFMEFI57 816X0197)].

References

1. Zuev D.A. et al. *Appl. Phys. B*, **105**, 545 (2011).
2. Tavera T., Perez N., Rodriguez A., Yurrita P., Olaisola S.M., Castano E. *Appl. Surf. Sci*., **258**, 1175 (2011).
3. Godbole V.P., Chaudhari S.M. *Bull. Mater. Sci*., **11**, 97 (1988).
4. Yang Q. et al. *Nano Lett*., **14**, 1769 (2014).
5. Vaccaro L., Sciortino L., Messina F., Buscarino G., Angello S., Cannas M. *Appl. Surf. Sci*., **302**, 62 (2014).
6. Aktsipetrov O.A., Baranova I.M., Evtyukhov K.N. *Nelineinaya optika kremniya i kremnievykh nanostruktur* (Nonlinear Optics of Silicon and Silicon Nanostructures) (Moscow: Fizmatlit, 2012).
7. Banishev A.F., Golubev V.S., Kremnev A.Yu. *Zh. Tekh. Fiz*., **71**, 33 (2001).
8. Banishev A.F., Golubev V.S., Kremnev A.Yu. *Pis'ma Zh. Tekh. Fiz*., **26**, 8 (2000).
9. Cracuin V., Bassim N., Singh R.K., Cracuin D., Hermann J., Boulmer-Leborgne C. *Appl. Surf. Sci*., **186**, 288 (2002).
10. O'Neil W., Li K. *IEEE J. Sel. Top. Quantum Electron*., **15**, 462 (2009).
11. Li K., Sparkes M., O'Neil W. *IEEE J. Sel. Top. Quantum Electron*., **20**, 900807 (2014).
12. Polyakov D.S., Sal'nikov N.M., Veiko V.P., Shimko A.A., Mikhailova A.A. *Izv. Vyssh. Uchebn. Zaved., Ser. Priborostroenie*, **60** (11), 1070 (2017).
13. Veiko V.P., Polyakov D.S., Skvortsov A.M., Chopenko E.S. *Pis'ma Zh. Tekh. Fiz*., **43**, 52 (2017).
14. Polyakov D., Skvortsov A., Veiko V. *J. Laser Micro/Nanoeng*., **10** (3), 269 (2015).
15. Skvortsov A.M., Veiko V.P., Huynh C.T., Polyakov D.S., Tamper A.M. *Quantum Electron*., **47** (6), 503 (2017) [*Kvantovaya Elektron*., **47** (6), 503 (2017)].
16. Huynh C.T. *Author's Abstract Dis. Cand.* (St. Petersburg, ITMO University, 2015).
17. Meyer J.R., Kruer M.R., Bartoli F.J. *J. Appl. Phys*., **51** (10), 5513 (1980).
18. Lietola A., Gibbons J.F. *J. Appl. Phys*., **53** (4), 3207 (1982).
19. Tao S., Zhou Y. *J. Appl. Phys*., **106**, 123507 (2009).
20. Tao S., Zhou Y., Benxin W., Gao Y. *Appl. Surf. Sci*., **258**, 7766 (2012).
21. Chernek P.J., Orson J.A. *Proc. SPIE*, **4679**, 186 (2002).

22. Verburg P.C., Romer G.R.B.E., Huisin't Veld A.J. *Appl. Phys. A*, **114**, 1135 (2014).
23. Kirichenko N.A., Kuz'min P.G., Shcherbina M.E. *Quantum Electron.*, **41**, 626 (2011) [*Kvantovaya Elektron.*, **41**, 626 (2011)].
24. Bonch-Bruevich A.M., Imas Ya.A., Libenson N.M., Salyadinov V.S., Shandybina G.D., Yakovlev E.B. *Zh. Tekh. Fiz.*, **47**, 609 (1977).
25. Libenson N.M. *Lazerno-indutsirovannye opticheskie i termicheskie protsessy v kondensirovannykh sredakh i ikh vzaimnoe vliyanie* (Laser-Induced Optical and Thermal Processes in Condensed Media and Their Mutual Influence) (St. Petersburg: Nauka, 2007).
26. Ashitkov S.I., Ovchinnikov A.V., Agranat M.B. *Pis'ma Zh. Eksp. Teor. Fiz.*, **79**, 657 (2004).
27. Gribkovskii V.P. *Teoriya pogloshcheniya i ispuskaniya sveta v poluprovodnikakh* (Theory of Light Absorption and Emission in Semiconductors) (Minsk: Nauka i tekhnika, 1975).
28. Berggren K.F., Sernelius B.E. *Phys. Rev. B*, **24** (4), 1971 (1981).
29. Vainshtein I.A., Zatsepin A.F., Kortov V.S. *Fiz. Tverd. Tela*, **41** (6), 994 (1999).
30. Grigoriev I.S., Meilikhov E.Z. *Handbook of Physical Quantities* (Boca Raton: CRC Press, 1996; Moscow: Energoatomizdat, 1991).
31. Monodane T., Ohmura E., Fukuyo F., Fukumitsu K., Morita H., Hirata Y. *JLMN*, **1** (3), 231 (2006).
32. Pankove J.I. *Optical Processes in Semiconductors* (Englewood Cliffs, N.J.: Prentice-Hall, 1971; Moscow: Mir, 1973).
33. Ramer A., Rethfeld B., Osmani O. *J. Appl. Phys.*, **116**, 053508 (2014).
34. Bogess T., Bohnert K., Mansour K., Moss S.C., Boyd I., Smirl A. *IEEE J. Quantum Electron.*, **22** (2), 360 (1986).
35. Chen S.C., Cahill D.G., Grigoropoulos C.P. *J. Heat Transfer*, **122**, 107 (2000).
36. Ma C., Ho W-Y., Walser R., Becker M. *Proc. SPIE*, **1848**, 59 (1992).
37. Samarskii A.A., Vabishchevich P.N. *Vychislitil'naya teploperedacha* (Computational Heat Transfer) (Moscow: Editorial URSS, 2003).